Thermal behavior as indicator for hyperons in binary neutron star merger remnants

Sebastian Blacker,[1,2] Hristijan Kochankovski,[3,4] Andreas Bauswein,[2,5] Angels Ramos,[3] and Laura Tolos[6,7,8]

[1]*Institut für Kernphysik, Technische Universität Darmstadt, 64289 Darmstadt, Germany*
[2]*GSI Helmholtzzentrum für Schwerionenforschung, Planckstraße 1, 64291 Darmstadt, Germany*
[3]*Departament de Física Quàntica i Astrofísica and Institut de Ciències del Cosmos, Universitat de Barcelona, Martí i Franquès 1, 08028 Barcelona, Spain*
[4]*Faculty of Natural Sciences and Mathematics-Skopje, Ss. Cyril and Methodius University in Skopje, Arhimedova, 1000 Skopje, North Macedonia*
[5]*Helmholtz Research Academy Hesse for FAIR (HFHF), Campus Darmstadt, 64291 Darmstadt, Germany*
[6]*Institute of Space Sciences (ICE, CSIC), Campus UAB, Carrer de Can Magrans, 08193 Barcelona, Spain*
[7]*Institut d'Estudis Espacials de Catalunya (IEEC), 08034 Barcelona, Spain*
[8]*Frankfurt Institute for Advanced Studies, Ruth-Moufang-Str. 1, 60438 Frankfurt am Main, Germany*

(Received 10 July 2023; accepted 21 January 2024; published 8 February 2024)

We provide the first comprehensive study of hyperons in neutron star mergers and quantify their specific impact. We discuss the thermal behavior of hyperonic equations of state (EOSs) as a distinguishing feature from purely nucleonic models in the remnants of binary mergers using a large set of numerical simulations. Finite temperature enhances the production of hyperons, which leads to a reduced pressure as highly degenerate nucleons are depopulated. This results in a characteristic increase of the dominant postmerger gravitational-wave frequency by up to ∼150 Hz compared to purely nucleonic EOS models. By our comparative approach we can directly link this effect to the occurrence of hyperons. Although this feature is generally weak, it is in principle measurable if the EOS and stellar parameters of cold neutron stars are sufficiently well-determined. Considering that the mass-radius relations of purely nucleonic and hyperonic EOSs may be indistinguishable and the overall challenge to infer the presence of hyperons in neutron stars, these findings are important as a new route to answer the outstanding question about hyperonic degrees of freedom in high-density matter.

DOI: 10.1103/PhysRevD.109.043015

I. INTRODUCTION

The "hyperon puzzle" states the apparent tension between the expectation that the occurrence of hyperons in dense nuclear matter would soften the equation of state (EOS) of neutron stars (NSs) and the observation that some NSs have about two solar masses, which thus requires a certain stiffness of the high-density EOS. Several modern EOS models including hyperons are compatible with these observations (see Refs. [1–29]). This is essentially achieved by tuning some parameters of the phenomenological mean-field models or by including the effect of three-body forces in the microscopical approaches. However, uncertainties remain since both the bare two-body and three-body interactions involving hyperons are poorly known. This is because the available data from scattering experiments are still scarce and subject to quite large error bars, although promising results are becoming available from final-state interaction analyses and femtoscopy studies [30–44]. Hypernuclear structure data can also provide indirect information about the hyperon nuclear forces [45–47]. For instance, recent systematic analyses of Λ separation energies in hypernuclei [48], as well as *ab initio* calculations of light Λ hypernuclei employing state-of-the-art chiral interactions [49–51], reveal the need for three-body forces involving hyperons that are expected to have an impact on the EOS around and above saturation density, hence on the properties and composition of neutron stars [23,25]. Unfortunately, the many-body treatment also contributes to the total uncertainty, although in the recent decade there has been a significant progress in this area [52–59]. The hyperon puzzle thus remains unsolved in the sense that to date it is still not clear whether hyperons are present in NSs.

Unless the problem can be solved self-consistently within many-body theory, i.e., including the precise knowledge of nucleon and hyperon interactions also at higher densities either from theory or experiment, which seems very ambitious, the solution of the hyperon puzzle necessarily requires the very accurate determination of the mass-radius relation of NSs.

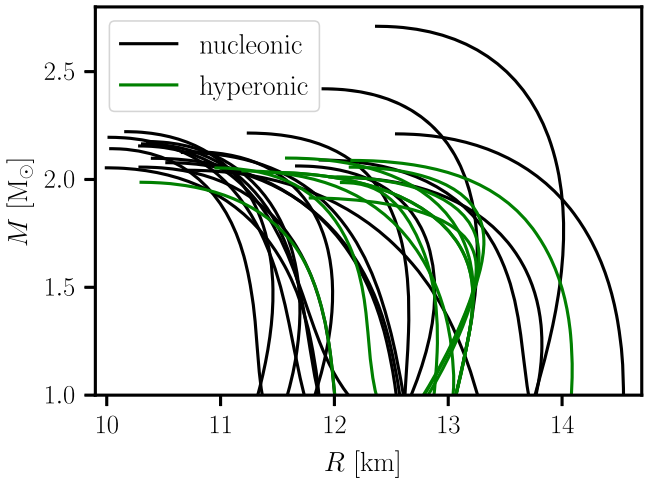

FIG. 1. Mass-radius relations for purely nucleonic (black) and hyperonic (green) EOSs considered in this study.

From stellar measurements one may either directly infer the presence of hyperons from some specific stellar features in a model-agnostic way or one may gain insights from a detailed comparison between theoretical expectations and observations. As both approaches still appear very challenging, it is justified to consider in this work the case that stellar parameters have been determined with very good precision, which may be achieved in future measurements, and to study which signature can then additionally reveal the presence of hyperons.

Comparing the mass-radius relations of hyperonic and nucleonic EOSs it is difficult to distinguish both classes (see Fig. 1) and hence it is not straightforward to tell from a measured mass-radius relation if the underlying EOS contains hyperons or not. This implies that even when the mass-radius relation of NSs is observationally determined with very good precision, it may still not be possible to deduce the presence of hyperons as no information on the composition can directly be inferred form the stellar parameters. This clearly shows that the identification of hyperonic degrees of freedom in NSs is very difficult and that additional features that may indicate the occurrence of hyperons are highly desirable to solve the hyperon puzzle even for the case that the mass-radius relation is observationally well-known.

In this paper we discuss a feature which can be clearly linked to the occurrence of hyperons in NS merger remnants and their associated postmerger gravitational wave (GW) emission; we identify the thermal behavior of hyperonic EOSs as a potential indicator for the presence of hyperons in NS mergers. Using a large set of numerical simulations we present here the first comprehensive study of hyperons in NS mergers that goes beyond comparing individual models (as in [60,61]), for which it may not be obvious if differences in the observables must be necessarily related to hyperons or could be similarly produced by another nucleonic model with similar EOS properties as the hyperonic model.[1] Reference [60] reports a difference in the main postmerger GW frequency comparing an EOS model with and without hyperons. In this work we consider all currently available temperature dependent hyperonic EOS models which are publicly accessible and roughly compatible with current astronomical constraints (see e.g., [75–99]). We find that the presence of hyperons at finite temperature leads to a small but systematic increase of the dominant postmerger GW frequency up to ∼150 Hz compared to purely nucleonic matter.

II. METHODS AND SETUP

We perform binary merger simulations using a general-relativistic, smoothed particle hydrodynamics (SPH) code [100–102] employing the conformal flatness condition to solve the field equations [103,104]. The effects of neutrinos and magnetic fields are not included. We consider equal- and nonequal-mass systems with a total binary mass of $M_{\rm tot} = 2.8 M_\odot$. The simulations start with cold, irrotational stars in neutrinoless beta-equilibrium on quasiequilibrium circular orbits with a center-to-center separation of 38 km. In the simulations we use two samples of EOS models. The first sample contains models that consider the occurrence of different species of hyperons and includes BHB$\Lambda\phi$ [105], DD2Y [106], DNS [107], FSU2H* [108], QMC-A [109], R(DD2YDelta)1.1-1.1 [7], R(DD2YDelta)1.2-1.1 [7], R(DD2YDelta)1.2-1.3 [7] and SFHOY [110]. We also consider two additional versions of the FSU2H* model, which approximately cover the range of uncertainties of hyperon potentials. Hyperons occur either at lower (FSU2H*L) or higher (FSU2H*U) densities compared to the original FSU2H* model see [111] for details). All of these EOSs are developed in the relativistic mean field framework, assuming a strongly repulsive vector meson contribution which is softened by considering density-dependent meson coupling constants or by introducing meson self-interactions. Three of the models, R(DD2YDelta)1.1-1.1, R(DD2YDelta)1.2-1.1 and R(DD2YDelta)1.2-1.3, also consider Δ resonances as an additional heavy baryon degree of freedom. The impact of Δ resonances on the EOS is analogous to those of the hyperons.

The second sample contains purely nucleonic EOSs that do not include exotic degrees of freedom. This sample

[1]As a side note we recall that GN3H and H4 are hyperonic $T = 0$ EOS models [62,63], which have often been used in merger simulations usually as piecewise polytropes [64] with approximate temperature treatment, e.g., [65–74]. To our knowledge no specific features distinguishing these models (qualitatively) from purely nucleonic models have been reported, which exemplifies the similarity between hyperonic and purely nucleonic models at $T = 0$.

TABLE I. Sample of EOSs considered in this work which include hyperonic degrees of freedom. Second to fifth column provide properties of cold stars, namely the maximum mass $M_{\max}$, the radius $R_{1.4}$ and tidal deformability $\Lambda_{1.4}$ of a $1.4M_\odot$ neutron star and the tidal deformability $\Lambda_{1.75}$ of a $1.75M_\odot$ neutron star. ρ_{onset} is the onset rest-mass density for the occurrence of hyperons in the $T = 0$, beta-equilibrium EOS slice and $\rho_{\text{init}}^{\max}$ corresponds to the maximum density in the system at the beginning of the simulation. Underlined values mark systems with hyperons present prior to the merger. Next two columns report the dominant postmerger GW frequency f_{peak} from simulations using either the full temperature-dependent EOS table or the barotropic EOS table together with the ideal-gas approximation for thermal pressure with $\Gamma_{\text{th}} = 1.75$. $\bar{\Gamma}_{\text{th}}$ and $\bar{Y}_{\text{hyp}}$ refer to the mass- and time-averaged thermal ideal-gas index and hyperon fraction of the remnant, respectively. $\rho^{\max}$ is the maximum rest-mass density within the first 5 ms after merger.

EOS	$M_{\max}$ [$M_\odot$]	$R_{1.4}$ [km]	$\Lambda_{1.4}$	$\Lambda_{1.75}$	ρ_{onset} ($T=0$) [10^{15} g/cm^3]	$\rho_{\text{init}}^{\max}$ [10^{15} g/cm^3]	f_{peak} (3D) [kHz]	f_{peak} ($\Gamma_{\text{th}}=1.75$) [kHz]	$\bar{\Gamma}_{\text{th}}$	$\bar{Y}_{\text{hyp}}$	$\rho^{\max}$ [10^{15} g/cm^3]	Ref.
BHB$\Lambda\phi$	2.10	13.21	695.2	160.1	0.56	<u>0.59</u>	2.76	2.68	1.37	0.018	0.79	[105]
DD2Y	2.03	13.21	694.8	150.9	0.56	<u>0.60</u>	2.82	2.73	1.08	0.022	0.80	[106]
DD2Y ($q = 0.8$)	2.03	13.21	694.8	150.9	0.56	<u>0.68</u>	2.76	2.63	1.04	0.050	1.00	[106]
DNS	2.09	14.04	957.7	208.3	0.77	0.55	2.51	2.54	1.69	0.003	0.66	[107]
FSU2H*	2.01	13.18	778.8	192.1	0.57	0.55	2.63	2.59	1.52	0.012	0.75	[108]
FSU2H* ($q = 0.8$)	2.01	13.18	778.8	192.1	0.57	<u>0.60</u>	2.76	2.69	1.37	0.025	0.87	[108]
FSU2H*L	1.91	13.16	784.4	177.6	0.56	0.54	2.68	2.62	1.24	0.018	0.76	[108,111]
FSU2H*U	2.06	13.17	784.4	205.7	0.58	0.54	2.62	2.56	1.51	0.008	0.70	[108,111]
QMC-A	1.99	12.89	574.8	126.0	0.93	0.66	2.91	2.98	1.65	0.003	0.91	[109]
R(DD2YDelta)1.1-1.1	2.04	12.96	586.8	114.0	0.46	<u>0.69</u>	3.03	2.93	1.08	0.083	0.95	[7]
R(DD2YDelta)1.2-1.1	2.05	12.27	397.3	85.4	0.37	<u>0.77</u>	3.26	3.14	1.18	0.185	1.16	[7]
R(DD2YDelta)1.2-1.3	2.03	13.21	696.1	150.8	0.56	<u>0.60</u>	2.82	2.72	0.99	0.029	0.84	[7]
SFHOY	1.99	11.89	333.6	61.9	0.97	0.85	3.60	3.46	1.38	0.015	1.54	[110]

consists of APR [112,113], DD2 [114,115], DD2F [114,116], FSU2R [21], FTNS [117,118], GS2 [119], LPB [120,121], LS220 [122], LS375 [122], SFHo [115,123], SFHx [115,123], SRO(SLy4) [124,125], TM1 [126,127] and TMA [127,128], and the models 'Fiducial', 'Large Mmax', 'Large SL', 'Large R', 'Small SL' and 'Smaller R' from Ref. [129].

All EOS models are available as fully temperature- and composition-dependent tables. Most of the EOSs are publicly available at the CompOSE website [2,130,131].[2] Some properties of cold, nonrotating NSs are summarized in Table I for the hyperonic EOS sample and Table II for the nucleonic one. With the adopted sets, we cover a broad range of stellar parameters roughly compatible with current constraints. All nucleonic EOSs and most of the hyperonic EOSs (except for FSU2H*L) reach a maximum mass above $\approx 2M_\odot$.

Note, however, that within the sample of hyperonic EOSs only BHB$\Lambda\Phi$ and DNS are compatible with the recent analysis in [97], i.e., $M_{\max} > 2.09M_\odot$ at the 3σ confidence level. Also the nucleonic EOSs DD2F, FSU2R, LS220, SFHo, SRO(Sly4) and TMA are in tension with this limit. The nucleonic models GS2, LS375, TM1 and TMA and the hyperonic models DNS, FSU2H*, FSU2H*L and, FSU2H*U are in conflict with the 90% credible level of the tidal deformability constraint from GW170817 [132–134]. We include these models in our analysis in order to have a larger sample to be used in simulations.

[2]https://compose.obspm.fr.

To analyze the thermal behavior of EOSs, we split the pressure P and specific internal energy ϵ into a cold and a thermal part, $P = P_{\text{cold}} + P_{\text{th}}$ and $\epsilon = \epsilon_{\text{cold}} + \epsilon_{\text{th}}$. The thermal components can be related through $P_{\text{th}} = (\Gamma_{\text{th}} - 1)\epsilon_{\text{th}}\rho$ adopting a thermal ideal-gas description with the thermal ideal-gas index Γ_{th} and rest-mass density ρ [135]. Γ_{th} is constant for an ideal gas but generally depends on density, temperature and composition for actual microphysical models (see e.g., [136] for details). The thermal ideal-gas approach can be employed if a temperature extension of microphysical EOS is not available [135,137]. The basic approximation consists in choosing a constant Γ_{th} with a value of ~ 1.75 reasonably reproducing the thermal behavior of purely nucleonic microphysical EOSs [137].

III. APPROACH AND RESULTS

Motivated by the fact that mass-radius relations of cold NSs can look very similar for nucleonic and hyperonic EOSs, we focus on the thermal EOS behavior. Therefore, we investigate the dominant postmerger GW frequency f_{peak}, which in contrast to observables of the binary inspiral phase is affected by finite-temperature effects [74,137–139]. To identify a clear signature of hyperons, we set up a numerical experiment to isolate the impact of the thermal behavior of EOSs.

For this we perform two sets of simulations with all EOS models. First, we run simulations using the full temperature- and composition-dependent EOS tables. For the other set of simulations, we adopt all EOSs at $T = 0$ in

TABLE II. Sample of purely nucleonic EOSs considered in this work. Second to fifth column provide properties of cold stars, namely the maximum mass $M_{\rm max}$, the radius $R_{1.4}$ and tidal deformability $\Lambda_{1.4}$ of a $1.4M_\odot$ neutron star and the tidal deformability $\Lambda_{1.75}$ of a $1.75M_\odot$ neutron star. Next two columns report the dominant postmerger GW frequency $f_{\rm peak}$ from simulations using either the full temperature-dependent EOS table or the barotropic EOS table together with the ideal-gas approximation for thermal pressure with $\Gamma_{\rm th} = 1.75$. $\bar{\Gamma}_{\rm th}$ refers to the mass- and time-averaged thermal ideal-gas index of the remnant. $\rho^{\rm max}$ is the maximum rest-mass density within the first 5 ms after merger.

EOS	$M_{\rm max}$ $[M_\odot]$	$R_{1.4}$ [km]	$\Lambda_{1.4}$	$\Lambda_{1.75}$	$f_{\rm peak}$(3D) [kHz]	$f_{\rm peak}$ ($\Gamma_{\rm th} = 1.75$) [kHz]	$\bar{\Gamma}_{\rm th}$	$\rho^{\rm max}$ [10^{15} g/cm^3]	Ref.
APR	2.20	11.57	267.6	54.5	3.51	3.46	1.74	1.41	[112,113]
DD2	2.42	13.22	698.8	178.5	2.64	2.68	1.78	0.71	[114,115]
DD2 ($q = 0.8$)	2.42	13.22	698.8	178.5	2.68	2.69	1.74	0.73	[114,115]
DD2F	2.08	12.40	425.5	79.3	3.30	3.30	1.66	1.12	[114,116]
DSH Fiducial	2.17	11.73	296.3	61.8	3.44	3.40	1.77	1.28	[129]
DSH Large Mmax	2.22	12.65	513.9	119.9	2.93	2.91	1.79	0.85	[129]
DSH Large SL	2.16	11.76	271.5	55.9	3.51	3.46	1.52	1.38	[129]
DSH Large R	2.13	12.44	437.6	87.3	3.16	3.18	1.72	1.08	[129]
DSH Small SL	2.18	11.70	335.8	70.3	3.31	3.33	1.76	1.21	[129]
DSH Smaller R	2.14	11.29	233.1	48.8	3.62	3.60	1.72	1.66	[129]
FSU2R	2.06	12.87	640.8	143.5	2.80	2.81	1.81	0.83	[21]
FSU2R ($q = 0.8$)	2.06	12.87	640.8	143.5	2.69	2.70	1.76	0.91	[21]
FTNS	2.22	11.46	304.8	65.3	3.34	3.40	1.73	1.26	[117,118]
GS2	2.09	13.60	721.3	160.6	2.73	2.70	1.76	0.73	[119]
LPB	2.10	12.37	429.9	79.9	3.23	3.23	1.68	1.01	[120,121]
LS220	2.04	12.96	541.9	94.2	3.09	3.06	1.54	1.00	[122]
LS375	2.71	13.95	960.1	257.7	2.44	2.44	1.63	0.59	[122]
SFHo	2.06	11.89	333.5	63.5	3.43	3.45	1.62	1.42	[115,123]
SFHx	2.13	11.98	395.1	86.7	3.16	3.18	1.82	1.09	[115,123]
SRO(SLy4)	2.05	11.72	303.7	54.7	3.51	3.50	1.78	1.43	[124,125]
TM1	2.21	14.47	1149.0	257.7	2.38	2.40	1.82	0.55	[126,127]
TMA	2.01	13.79	929.1	184.1	2.58	2.57	1.74	0.66	[127,128]

neutrinoless beta-equilibrium and assume that all these barotropic EOSs would result from purely nucleonic matter.[3] We supplement these barotropic models with the ideal-gas treatment of thermal pressure with $\Gamma_{\rm th} = 1.75$. This choice mimics the thermal behavior of purely nucleonic matter (as confirmed below), i.e., we equip also the cold hyperonic models with a thermal part characteristic of purely nucleonic matter.

In the simulations using the full EOS table the lepton fraction Y_e of each fluid element is determined by cold beta-equilibrium in the setup of the two stars and then advected during the simulation as we do not consider neutrinos. In the simulations employing the barotropic EOS slice with the ideal gas approach the lepton fraction is always set to the cold beta-equilibrium value at the respective density (see [137] for a discussion). The hyperon content is always assumed to be in weak equilibrium.

[3]We here assume that the function $P(\rho)$ for a given cold hyperonic EOS could be similarly produced by different nucleonic interactions within a purely nucleonic model.

To also test asymmetric systems we perform additional simulations with a total binary mass of $2.8M_\odot$ and a mass ratio of $q = 0.8$ using the hyperonic models DD2Y and FSU2H* and the nucleonic EOSs DD2 and FSU2R with both thermal schemes.

We summarize our simulation results and stellar properties from both sets of simulations in Table I and Table II for the hyperonic and the nucleonic EOS sample, respectively. For hyperonic models we also provide the onset rest-mass density $\rho_{\rm onset}$ of hyperons in neutrinoless beta-equilibrium matter at zero temperature as well as the maximum density in the system at the start of the simulation. Underlined values mark systems where hyperons are already present prior to the merger. Tables I and II also report the mass- and time-average values of the thermal ideal-gas index $\bar{\Gamma}_{\rm th}$ and the hyperon fraction $\bar{Y}_{\rm hyp}$ extracted from the simulations employing the fully temperature-dependent EOSs. For $\bar{\Gamma}_{\rm th}$ we first determine a mass-averaged value $\Gamma_{\rm th}^{\rm av} = \sum m_i \Gamma_{{\rm th},i} / \sum m_i$. Here quantities with an index refer to local quantities of a single SPH particle i. For particles with a temperature equal to the lowest T in the EOS table (typically 0.1 MeV) we set $\Gamma_{{\rm th},i} = 1$. We then average

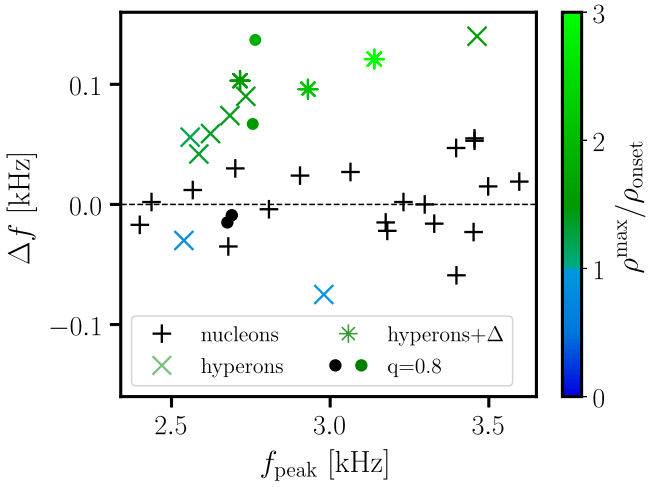

FIG. 2. Difference $\Delta f = f_{\rm peak} - f^{1.75}_{\rm peak}$ between dominant postmerger GW frequency of simulations with fully temperature-dependent EOSs and calculations with same EOS models restricted to zero temperature and supplemented with an ideal-gas treatment of thermal effects, which mimics the behavior of purely nucleonic EOSs by choosing a thermal ideal-gas index of $\Gamma_{\rm th} = 1.75$. Shown as function of $f_{\rm peak}$. Black symbols depict purely nucleonic models. Crosses display hyperonic models, where the coloring indicates the ratio between the maximum rest-mass density in the postmerger remnant and the onset rest-mass density of hyperon production at zero temperature. Asterisks refer to models which additionally include Δ-baryons. Circles display results from asymmetric binaries.

$\Gamma^{\rm av}_{\rm th}$ in a time window of 5 ms starting at 2.5 ms after merger. $\bar{Y}_{\rm hyp}$ is calculated analogously.

We now compare the dominant postmerger GW frequencies of the full models, $f_{\rm peak}$, with the frequencies $f^{1.75}_{\rm peak}$ obtained from the $\Gamma_{\rm th} = 1.75$ calculations. The difference $\Delta f \equiv f_{\rm peak} - f^{1.75}_{\rm peak}$ describes how well the thermal behavior of the full EOS table is modeled by $\Gamma_{\rm th} = 1.75$ and thus measures by how much a given model deviates from an idealized "nucleonic" thermal behavior. The results are given in Fig. 2, where we distinguish purely nucleonic models (black) and hyperonic models (colored). As anticipated, the purely nucleonic models cluster around zero corroborating that $\Gamma_{\rm th} = 1.75$ is a good choice for nucleonic matter (but see discussion below). Hyperonic models lead to systematically higher frequencies compared to the $\Gamma_{\rm th} = 1.75$ runs, which mimic a nucleonic behavior.

The color of the symbols in Fig. 2 indicates by how much the maximum rest-mass density in the merger remnant within the first 5 ms after the merger, $\rho^{\rm max}$, exceeds the rest-mass density $\rho_{\rm onset}$ where hyperons occur in cold matter for the given EOS. Models with $\rho^{\rm max}/\rho_{\rm onset} < 1$ still contain a tiny amount of hyperons due to their occurrence at finite temperature (about 0.3%; see Table I). The coloring in Fig. 2 looks very similar if we choose it to directly indicate the hyperon content in the remnant or a mass-averaged thermal ideal-gas index since these two quantities correlate with $\rho^{\rm max}/\rho_{\rm onset}$. Obviously, if only a very small amount of hyperons is present, hardly any impact on the dominant postmerger frequency is expected, which is why two blue symbols in Fig. 2 are located around $\Delta f \sim 0$ as the nucleonic models. We also remark that the results from the asymmetric binaries are in good agreement with the findings from symmetric systems.

A frequency shift of $f_{\rm peak}$ of about 100 Hz is small (compared to the FWHM of the peaks or the variation of $f_{\rm peak}$ with the EOS) but potentially sizable enough for a detection. Clearly, a frequency shift itself cannot be measured directly since only one true neutron star EOS exists. We envision a scenario where an observed $f_{\rm peak}$ has to be compared to simulation results with different thermal approaches.

In other words, suppose the cold EOS was known with good precision (e.g., from GW inspiral measurements), but the actual content of the matter—whether hyperons are present or not—remains unknown. This degeneracy is broken by thermal effects, which influence $f_{\rm peak}$. One can then perform merger simulations to predict a reference value, $f^{1.75}_{\rm peak}$ using the cold EOS and the ideal-gas approach with $\Gamma_{\rm th} = 1.75$, i.e., a typical thermal behavior for purely nucleonic matter. A deviation between $f^{1.75}_{\rm peak}$ and the actually measured $f_{\rm peak}$ by around 50 Hz to 150 Hz would indicate the presence of hyperons.

Gravitational-wave injection studies as in [140–148] show that $f_{\rm peak}$ may be determined to within ∼10 Hz by future facilities such that a frequency shift of this order is in principle measurable and thus the effect of hyperons would be accessible.

However, this requires not only the cold EOS to be measured sufficiently well but, additionally, that simulation tools are reliable enough to predict an accurate reference value $f^{1.75}_{\rm peak}$ for the comparison with the observational data. Both prerequisites are currently not given but might be achieved in the future albeit they clearly represent challenging efforts. To provide a coarse estimate of the requirements we note that a frequency shift of 100 Hz corresponds to a change of the NS radius of about 250 m considering empirical relations that connect $f_{\rm peak}$ and the radius of cold, nonrotating NSs [149].

Another potentially very promising route to identify the presence of hyperons links two directly measurable quantities. Importantly, this detection scenario does not assume that the cold EOS is known. Employing the same simulation data, we relate $f_{\rm peak}$ and the tidal deformability Λ. The tidal deformability describing finite-size effects during the GW inspiral is given by $\Lambda = \frac{2}{3} k_2 (\frac{R}{M})^5$ with the stellar mass and radius, M and R, and the tidal Love number k_2 being a function of mass and the EOS [150–154]. As the stellar radius, Λ characterizes the cold EOS and it can be measured during the GW inspiral phase (see, e.g., [84,132,155,156]).

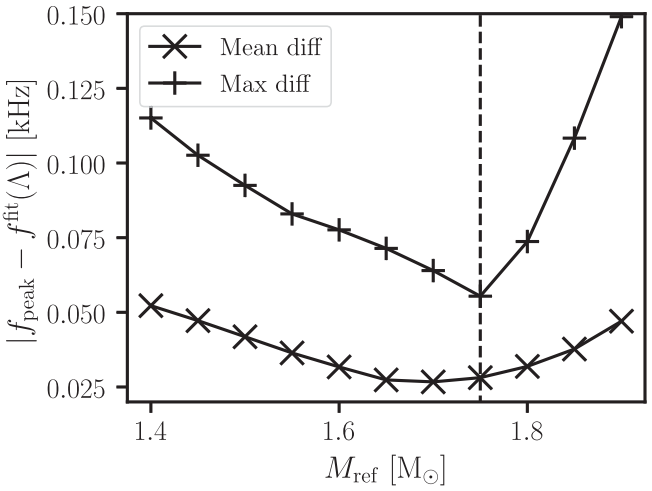

FIG. 3. Mean and maximum deviation of our data for purely nucleonic EOSs from quadratic $f_{\rm peak} - \Lambda_M$ least-squares fits for different reference masses $M_{\rm ref}$ at which Λ is evaluated [$\Lambda_M = \Lambda(M_{\rm ref})$]. The dashed vertical line indicates the minimum of the largest deviation at $M_{\rm ref} = 1.75$.

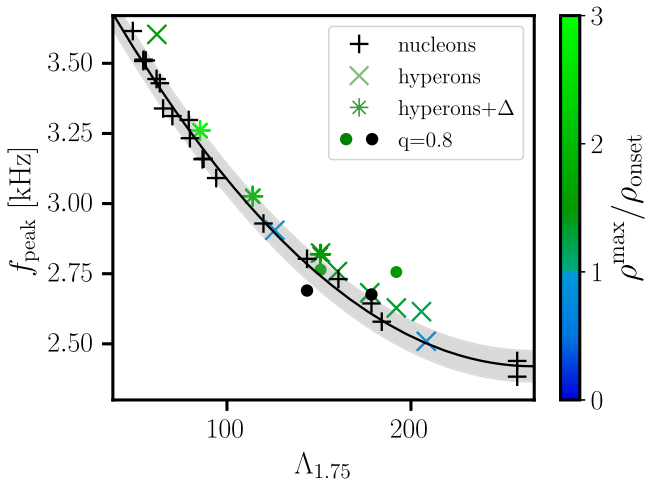

FIG. 4. Dominant postmerger GW frequency of $1.4M_\odot$–$1.4M_\odot$ mergers as function of tidal deformability of a $1.75M_\odot$ NS. Symbols and color scheme as in Fig. 2. Black curve shows least-squares fit to purely nucleonic models. Gray band indicates maximum residual of purely nucleonic models from the fit.

Given that we consider $1.4M_\odot$–$1.4M_\odot$ binaries a natural choice would be to relate $f_{\rm peak}$ to the tidal deformability $\Lambda_{1.4}$ of a $1.4M_\odot$ star. However, when relating $f_{\rm peak}$ and Λ, the reference mass $M_{\rm ref}$ at which Λ is evaluated can be in principle chosen freely but the choice affects the accuracy of the relation [157].

Similar to Ref. [157], in Fig. 3 we plot the mean and the maximum deviation of our data for purely nucleonic EOSs from the quadratic $f_{\rm peak} - \Lambda_M$ fit for different $M_{\rm ref}$ with $\Lambda_M = \Lambda(M_{\rm ref})$. As expected we find that the scatter depends on $M_{\rm ref}$. The maximum deviation reaches a minimum of 55 Hz at $M_{\rm ref} = 1.75M_\odot$, indicated by the vertical dashed line. Since this relation has the smallest overall scatter, we compare the results from the hyperonic EOS sample to this relation.

In Fig. 4 we display $f_{\rm peak}$ from the simulations with the fully temperature-dependent EOSs as function of the tidal deformability of $1.75M_\odot$ NSs. The black line is a least-squares quadratic fit to the purely nucleonic models and those data points deviate at most by 55 Hz from the fit. The average deviation of nucleonic models is only 28 Hz. As suggested by Fig. 2 the dominant postmerger frequency of hyperonic models (colored symbols) is characteristically increased compared to the nucleonic models. Most hyperonic models lie above the frequency range which is spanned by the fit to nucleonic models and the maximum residual of nucleonic models (visualized by the gray band). This implies that at least in principle the presence of hyperons may be deduced by an increased postmerger frequency which is incompatible with a purely nucleonic EOS. On the other hand, hyperon content up to a certain density (see Fig. 8 in [158]) may be excluded if inferred values of $\Lambda_{1.75}$ and $f_{\rm peak}$ lie below the fit to purely nucleonic models. Obviously, this scenario relies on simulations being sufficiently accurate in predicting $f_{\rm peak}$ for a given EOS. Again simulations where only a small amount of hyperons is present (blue symbols), lie practically on top of the fit to nucleonic EOSs. For the two asymmetric binaries with nucleonic EOSs we observe a somewhat larger scatter from the relation. This could imply that a different reference mass should be used for these systems or that $f_{\rm peak} - \Lambda$ relations are simply not as tight in the case of asymmetric binaries. This should be further investigated in future work.

Some models with a sizable fraction of hyperons do not stick out very clearly due to the overall properties of their EOS. These hyperonic models do result in a significant frequency shift by the thermal behavior of the hyperons, as can be seen in Fig. 2. However, this shift essentially only compensates the fact that the fiducial "nucleonic" models (i.e., with $\Gamma_{\rm th} = 1.75$) produce relatively low frequencies in Fig. 4, i.e., close to the lower edge of the gray band. This can be seen by the frequency shift of the respective model in Fig. 2.

This shows that it is not straightforward to connect the exact location of a hyperonic model with respect to the fit in Fig. 4 with the actual amount of hyperons in the remnant, albeit one may generally conclude that the presence of hyperons seems more likely if the postmerger frequency is high compared to the fit. The exact location is a superposition of the thermal behavior and properties of the cold EOS which are not captured by $\Lambda_{1.75}$. Our set of EOSs does not represent a statistical ensemble and one should thus be careful with likelihood arguments.

Since the magnitude of the frequency shift of hyperonic models is generally small, the intrinsic scatter of $f_{\rm peak}(\Lambda)$ relations is particularly relevant and a better understanding of the scatter of such empirical relations will improve the prospects to infer the presence of hyperons.

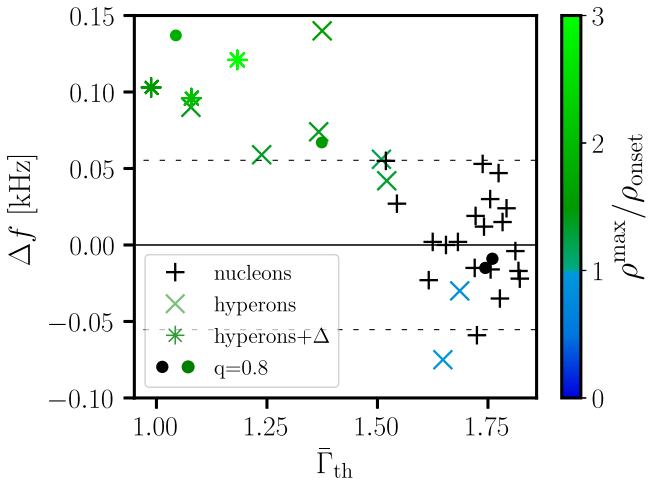

FIG. 5. Difference $\Delta f = f_{\rm peak} - f_{\rm peak}^{1.75}$ as function of mass- and time-averaged thermal index of the merger remnant in simulations employing the temperature-dependent EOSs. Same symbols and color scheme as in Fig. 2. Dashed lines indicate maximum residual of $f_{\rm peak} - \Lambda_{1.75}$ fit to purely nucleonic EOSs from Fig. 4.

Figure 5 illustrates the dependence of GW frequency shifts Δf on mass-averaged and time-averaged ideal-gas index $\bar{\Gamma}_{\rm th}$. As in Fig. 2 we also include some results for asymmetric binaries. The figure clearly shows that the presence of hyperons leads to a reduction of the thermal pressure component in comparison to purely nucleonic models. The increase of the thermal energy favors the occurrence of hyperons, which, in turn, reduces pressure from the highly degenerate species resulting in a substantial decrease of the thermal index. The figure also summarizes

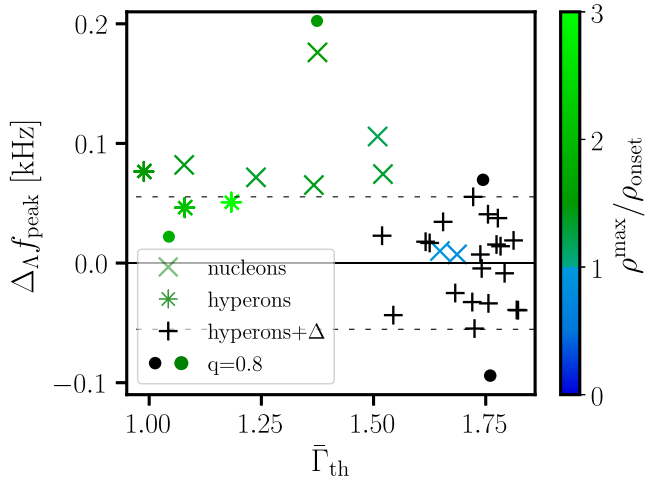

FIG. 6. Difference between the dominant postmerger GW frequency of $1.4M_\odot$–$1.4M_\odot$ mergers and the frequency given by the least-squares fit of $f_{\rm peak}(\Lambda_{175})$ for hyperonic and purely nucleonic models (see Fig. 4) as function of the mass- and time averaged thermal ideal-gas index of the remnant. Same symbols and color scheme as in Fig. 2. Dashed lines indicate maximum residual of the fit to purely nucleonic EOSs.

the observation that many of the hyperonic models feature a frequency shift that is larger than the maximum residual of the fit to nucleonic models in Fig. 4. Figure 5 also demonstrates that $\Gamma_{\rm th} = 1.75$ is a good choice to model the thermal behavior of nucleonic EOSs.

Additionally, in Fig. 6 we visualize the deviations from the $f_{\rm peak} - \Lambda_{1.75}$ relation for purely nucleonic models as a function of the mass- and time-averaged thermal ideal-gas index $\bar{\Gamma}_{\rm th}$ for purely nucleonic and hyperonic EOSs. Again, we observe that for most hyperonic EOS models the deviation from the relation is comparable or slightly above the maximum residual of the relation for purely nucleonic models. Since the magnitude of the frequency deviation from the fit is influenced by both the properties of the cold and the finite-temperature EOS, the deviations do not exactly scale with $\bar{\Gamma}_{\rm th}$ or $\rho^{\rm max}/\rho_{\rm onset}$.

IV. TOY MODEL: THERMAL BEHAVIOR OF HYPERONS

In recent studies based on chiral effective field theory (χEFT) for nucleons [159,160] a drop of the thermal index with density is observed. In these state-of-the art calculations for nuclear matter, the thermal pressure is reduced with density due to the increase of the effective nucleon mass. This stems from the strong three body force within χEFT, which in turn reduces the thermal index [see Eq. (41) in Ref. [159]]. However, χEFT in dense nuclear matter is applicable for densities up to around $2n_0$ (n_0 being the nuclear saturation density) and temperature $T \lesssim 30$ MeV [57] and, therefore, the resulting EOS cannot be used directly in NS merger simulations. Moreover, up to now, the above χEFT finite-temperature framework does not include exotic degrees of freedom, such as hyperons.

If the drop of the thermal index as predicted within χEFT [159,160] is a generic feature within a larger density range, this property could mimic the thermal behavior of hyperons as discussed in this work. We therefore explore, within a toy model that shows a similar drop of the thermal index in nucleonic matter as that of the phenomenological extrapolation of the microscopic χEFT model performed in [161], what would be the additional effect of the hyperonic degrees of freedom. To this end we build a toy model within the relativistic mean-field framework, adopting the DDME2 model [162] extended to the hyperonic sector with the density-dependent couplings as defined in [163]. We impose a similar drop of the thermal index in purely nucleonic matter as that in [161] by modifying the functional density dependence of the σ-meson coupling for nucleons, such that their effective mass experiences a minimum close to n_0. Other meson couplings remain unchanged. We stress that the EOS constructed in this way is not compatible with nuclear physics constraints, coming from the properties of nuclear matter, nuclei,

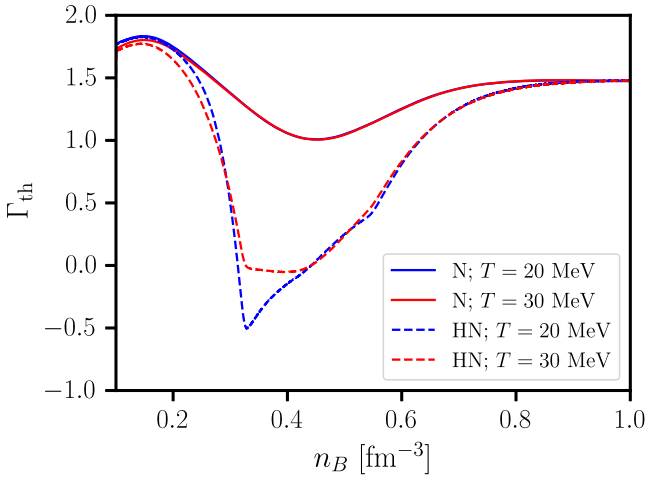

FIG. 7. The thermal index for nucleonic (solid lines) and hyperonic matter (dashed lines) for two different temperatures, $T = 20$ MeV (blue lines) and $T = 30$ MeV (red lines). See text for details of the model.

heavy ion collisions at high energies and astrophysical observations (see, for example, reviews on the EOS and the nuclear and astrophysical constraints of Refs. [3,5,164]). This setup just provides a purely nucleonic model with a thermal index sensibly below $\Gamma_{\rm th} = 4/3$, allowing us to additionally include hyperons and analyze their thermal effects. This is meant to resemble the aforementioned behavior found in the χEFT framework but with the inclusion of hyperons.

From Fig. 7 one can see that the occurrence of hyperons in β^- equilibrated matter at densities above 0.2 fm^{-3} gives rise to a significantly stronger reduction of the thermal index than in the nucleonic case. Similarly to the EOS models employed in this work, this additional drop of the thermal index is due to the loss of degeneracy pressure as hyperons appear, a mechanism that is apparently present regardless of the underlying nucleonic interaction.

However, a few words of caution are in order. As already mentioned, this toy model does not reproduce neither nuclear matter properties nor astrophysical observations, and therefore a more realistic simulation should be investigated in future work. We also note that in the relativistic-mean-field scheme employed to build our toy model the effective masses of hyperons are correlated with the nucleonic ones, as the coupling constants for nucleons and hyperons are related by symmetry relations. This implies that the effective masses of the nucleons and hyperons have the same functional dependence, which is not necessarily the case, and this may have an influence on the size of the additional hyperonic drop. As these questions are beyond the scope of the present work, based on the results of this study we can simply conclude that even if a nucleonic model would have rather low values of the thermal index, one should expect an additional decrease due to the occurrence of hyperons.

V. SUMMARY AND DISCUSSION

We conclude this work by discussing the prospects of identifying hyperons in NSs through their thermal properties as well as the possible caveats. By the approach chosen in this study we for the first time isolate the specific impact of the thermal behavior of hyperons in NS mergers. Above we already discussed caveats and challenges of identifying hyperons through their thermal behavior like requiring very precise stellar measurements (e.g., of $\Lambda_{1.75}$) and accurate simulations for reference. We have motivated and justified these rather optimistic assumptions by the difficulties to otherwise obtain information about the presence of hyperons in NSs. Any attempt to infer the presence of hyperons through astronomical measurements similarly requires very high or even higher precision to decipher their very weak impact on the stellar structure. Therefore, any new, additional feature which can be linked to hyperons as the one discussed in this paper is highly valuable. A few more comments on the prospects and caveats are in order.

We here explicitly assumed that the properties of the cold EOS and of cold, isolated NSs do not carry any information on the presence of hyperons. This was necessary to neatly quantify the impact of hyperons on the thermal behavior, but this is a very conservative and in fact incorrect assumption. In reality the cold EOS and NS parameters are affected by hyperons and for instance theoretical calculations of purely nucleonic matter may in future already indicate the presence of additional degrees of freedom when compared to measurements of cold NSs. Also advances on the experimental determination of two-body and three-body interactions involving hyperons and nucleons, e.g., at J-PARC, LHC or the future FAIR facility, and corresponding theoretical progress can be anticipated [33–42,165–168], which would lead to further constraints that can be incorporated in future analyses. *Ab initio* calculations that consider hyperons as relevant degrees of freedom may furthermore constrain the parameter space [49,50,169,170]. Further insights may result from astronomical observations like cooling NSs or core-collapse supernovae [1,6,8,171–183]. We also note that recent studies have shown significant progress in measuring NS properties and determining the EOS partially employing statistical methods to combine different measurements and by this to decrease uncertainties (see e.g., [75–99]).

We already discussed above that the exact frequency shift will depend on the abundance of hyperons and thus on the threshold density for hyperon production. Smaller amounts corresponding to a high threshold density of hyperonization may not lead to strong effects and may thus remain undetected. The amount of hyperons produced will also depend on the mass of the system. One may generally expect that the impact of hyperons becomes more pronounced for more massive systems. In this work we have only considered a single system mass, since once $f_{\rm peak}$ can be measured with sufficient precision, the binary mass

will be inferred with high accuracy. The increase of f_{peak} with the total binary mass can be estimated from Fig. 1 of Ref. [184] showing that a mass uncertainty of about 0.1% corresponds to a change of f_{peak} of a few Hz, which is well below frequency shifts induced by the thermal behavior of hyperonic EOSs. We also emphasize that a frequency shift incompatible with purely nucleonic matter, does not necessarily indicate the presence of hyperons but more generally degrees of freedom that lead to a softening of the EOS. This includes in particular the possibility of deconfined quark matter as discussed in [158,185–189]. Pions may additionally affect the EOS [190]. Likely, additional information from either theory or experiments in the laboratory is essential to discriminate these possibilities. We also refer to recent studies indicating the possibility that the thermal behavior of purely nucleonic matter may yield reduced thermal pressure, i.e., with a Γ_{th} significantly below 1.75, possibly even below 1 corresponding to negative thermal pressure [159,160]. These state-of-the-art microscopic models cannot be used directly in simulations since they only produce results up to around two times nuclear saturation density (see [74,137–139] for an exploration of thermal EOS effects in mergers). Phenomenological models developed to extrapolate these microscopic EOSs indicate that the thermal index reaches again larger values at higher densities [161], which may lead to an average thermal index inside the star that is close to the usual nucleonic values adopted here. Furthermore, the inclusion of hyperons in nucleonic models with low-average thermal index may still yield an additional softening of the thermal part of the EOS such that a very similar frequency shift relative to these nucleonic models may occur. We corroborate this argument with a toy model where we add hyperons to a model that we tuned such that the nucleonic part already features a drop in Γ_{th}.

A solid interpretation of a possible frequency shift in a future detection will at any rate require a comprehensive comparison with advanced theoretical models and other insight from upcoming astronomical and laboratory measurements.

ACKNOWLEDGMENTS

We thank K. Chatziioannou for comments on the manuscript. H. K. and A. R. would like to thank Arnau Rios for useful discussions. We acknowledge funds by the State of Hesse within the Cluster Project ELEMENTS supporting H. K.'s visit during which this project was initialized. This research has been supported from the projects CEX2019-000918-M, CEX2020-001058-M (Unidades de Excelencia "María de Maeztu"), PID2019-110165GB-I00, PID2020-118758GB-I00, and PID2022-139427NB-I00, financed by the Spanish Ministry for Science and Innovation—MCIN/AEI/10.13039/501100011033/ FEDER,UE, as well as by the EU STRONG-2020 project, under the program H2020-INFRAIA-2018-1 Grant Agreement No. 824093, and by PHAROS COST Action No. CA16214. H. K. acknowledges support from the PRE2020-093558 Doctoral Grant of the spanish MCIN/AEI. S. B. and A. B. acknowledge support by Deutsche Forschungsgemeinschaft (DFG, German Research Foundation) through Project No. 279384907—SFB 1245 (subproject B07). A. B. acknowledges support by the European Research Council (ERC) under the European Union's Horizon 2020 research and innovation program under Grant Agreement No. 759253 and ERC Grant HEAVYMETAL No. 101071865 and support by the State of Hesse within the Cluster Project ELEMENTS. L. T. also acknowledges support from the Generalitat Valenciana under Contract No. PROMETEO/2020/023, from the Generalitat de Catalunya under Contract No. 2021 SGR 171, and from the CRC-TR 211 'Strong-interaction matter under extreme conditions'- Project No. 315477589—TRR 211.

[1] D. Chatterjee and I. Vidaña, Do hyperons exist in the interior of neutron stars?, Eur. Phys. J. A **52**, 29 (2016).
[2] M. Oertel, M. Hempel, T. Klähn, and S. Typel, Equations of state for supernovae and compact stars, Rev. Mod. Phys. **89**, 015007 (2017).
[3] L. Tolos and L. Fabbietti, Strangeness in nuclei and neutron stars, Prog. Part. Nucl. Phys. **112**, 103770 (2020).
[4] J. Schaffner-Bielich, *Compact Star Physics* (Cambridge University Press, Cambridge, England, 2020).
[5] G. F. Burgio, H. J. Schulze, I. Vidana, and J. B. Wei, Neutron stars and the nuclear equation of state, Prog. Part. Nucl. Phys. **120**, 103879 (2021).
[6] A. Sedrakian, J.-J. Li, and F. Weber, Hyperonization in compact stars, in *Astrophysics in the XXI Century with Compact Stars*, edited by C. A. Z. Vasconcellos (World Scientific, Singapore, 2022), pp. 153–199, ISBN: 978-981-12-2094-4.
[7] A. R. Raduta, Equations of state for hot neutron stars-II. The role of exotic particle degrees of freedom, Eur. Phys. J. A **58**, 115 (2022).
[8] A. Sedrakian, J.-J. Li, and F. Weber, Heavy baryons in compact stars, Prog. Part. Nucl. Phys. **131**, 104041 (2023).
[9] T. Takatsuka, S. Nishizaki, and R. Tamagaki, Three-body force as an 'extra repulsion' suggested from

hyperon-mixed neutron stars, Prog. Theor. Phys. Suppl. **174**, 80 (2008).
[10] I. Bednarek, P. Haensel, J. L. Zdunik, M. Bejger, and R. Manka, Hyperons in neutron-star cores and two-solar-mass pulsar, Astron. Astrophys. **543**, A157 (2012).
[11] S. Weissenborn, D. Chatterjee, and J. Schaffner-Bielich, Hyperons and massive neutron stars: Vector repulsion and SU(3) symmetry, Phys. Rev. C **85**, 065802 (2012); Phys. Rev. C **90**, 019904(E) (2014).
[12] L. Bonanno and A. Sedrakian, Composition and stability of hybrid stars with hyperons and quark color-superconductivity, Astron. Astrophys. **539**, A16 (2012).
[13] J. L. Zdunik and P. Haensel, Maximum mass of neutron stars and strange neutron-star cores, Astron. Astrophys. **551**, A61 (2013).
[14] Y. Yamamoto, T. Furumoto, N. Yasutake, and T. A. Rijken, Hyperon mixing and universal many-body repulsion in neutron stars, Phys. Rev. C **90**, 045805 (2014).
[15] D. Lonardoni, A. Lovato, S. Gandolfi, and F. Pederiva, Hyperon puzzle: Hints from quantum Monte Carlo calculations, Phys. Rev. Lett. **114**, 092301 (2015).
[16] A. Drago, A. Lavagno, G. Pagliara, and D. Pigato, Early appearance of Δ isobars in neutron stars, Phys. Rev. C **90**, 065809 (2014).
[17] K. A. Maslov, E. E. Kolomeitsev, and D. N. Voskresensky, Solution of the hyperon puzzle within a relativistic mean-field model, Phys. Lett. B **748**, 369 (2015).
[18] A. Drago, A. Lavagno, G. Pagliara, and D. Pigato, The scenario of two families of compact stars: 1. Equations of state, mass-radius relations and binary systems, Eur. Phys. J. A **52**, 40 (2016).
[19] M. Oertel, F. Gulminelli, C. Providência, and A. R. Raduta, Hyperons in neutron stars and supernova cores, Eur. Phys. J. A **52**, 50 (2016).
[20] L. Tolos, M. Centelles, and A. Ramos, Equation of state for nucleonic and hyperonic neutron stars with mass and radius constraints, Astrophys. J. **834**, 3 (2017).
[21] L. Tolos, M. Centelles, and A. Ramos, The equation of state for the nucleonic and hyperonic core of neutron stars, Pub. Astron. Soc. Aust. **34**, e065 (2017).
[22] M. Fortin, S. S. Avancini, C. Providência, and I. Vidaña, Hypernuclei and massive neutron stars, Phys. Rev. C **95**, 065803 (2017).
[23] D. Logoteta, I. Vidana, and I. Bombaci, Impact of chiral hyperonic three-body forces on neutron stars, Eur. Phys. J. A **55**, 207 (2019).
[24] P. Ribes, A. Ramos, L. Tolos, C. Gonzalez-Boquera, and M. Centelles, Interplay between Δ particles and hyperons in neutron stars, Astrophys. J. **883**, 168 (2019).
[25] D. Gerstung, N. Kaiser, and W. Weise, Hyperon–nucleon three-body forces and strangeness in neutron stars, Eur. Phys. J. A **56**, 175 (2020).
[26] D. Logoteta, Hyperons in neutron stars, Universe **7**, 408 (2021).
[27] T. Malik, S. Banik, and D. Bandyopadhyay, Equation-of-state table with hyperon and antikaon for supernova and neutron star merger, Astrophys. J. **910**, 96 (2021).
[28] T. Muto, T. Maruyama, and T. Tatsumi, Effects of three-baryon forces on kaon condensation in hyperon-mixed matter, Phys. Lett. B **820**, 136587 (2021).
[29] V. B. Thapa, M. Sinha, J. J. Li, and A. Sedrakian, Massive Δ-resonance admixed hypernuclear stars with antikaon condensations, Phys. Rev. D **103**, 063004 (2021).
[30] V. M. Shapoval, B. Erazmus, R. Lednicky, and Y. M. Sinyukov, Extracting $p\Lambda$ scattering lengths from heavy ion collisions, Phys. Rev. C **92**, 034910 (2015).
[31] J. Adamczewski-Musch *et al.* (HADES Collaboration), The **Λp** interaction studied via femtoscopy in p + Nb reactions at $\sqrt{s_{NN}} = 3.18$ **GeV**, Phys. Rev. C **94**, 025201 (2016).
[32] L. Adamczyk *et al.* (STAR Collaboration), ΛΛ correlation function in Au + Au collisions at $\sqrt{s_{NN}} = 200$ GeV, Phys. Rev. Lett. **114**, 022301 (2015).
[33] J. Rowley *et al.* (CLAS Collaboration), Improved Λp elastic scattering cross sections between 0.9 and 2.0 GeV/c and connections to the neutron star equation of state, Phys. Rev. Lett. **127**, 272303 (2021).
[34] K. Miwa *et al.* (J-PARC E40 Collaboration), Measurement of the differential cross sections of the $\Sigma^- p$ elastic scattering in momentum range 470 to 850 MeV/c, Phys. Rev. C **104**, 045204 (2021).
[35] K. Miwa *et al.* (J-PARC E40 Collaboration), Precise measurement of differential cross sections of the $\Sigma^- p \to \Lambda n$ reaction in momentum range 470–650 MeV/c, Phys. Rev. Lett. **128**, 072501 (2022).
[36] T. Nanamura *et al.* (J-PARC E40 Collaboration), Measurement of differential cross sections for Σ + p elastic scattering in the momentum range 0.44–0.80 GeV/c, Prog. Theor. Exp. Phys. **2022**, 093D01 (2022).
[37] S. Acharya *et al.* (ALICE Collaboration), p-p, p-Λ and Λ-Λ correlations studied via femtoscopy in pp reactions at $\sqrt{s} = 7$ TeV, Phys. Rev. C **99**, 024001 (2019).
[38] S. Acharya *et al.* (ALICE Collaboration), Study of the Λ-Λ interaction with femtoscopy correlations in pp and p-Pb collisions at the LHC, Phys. Lett. B **797**, 134822 (2019).
[39] S. Acharya *et al.* (ALICE Collaboration), Investigation of the p − Σ0 interaction via femtoscopy in pp collisions, Phys. Lett. B **805**, 135419 (2020).
[40] S. Acharya *et al.* (ALICE Collaboration), First observation of an attractive interaction between a proton and a cascade baryon, Phys. Rev. Lett. **123**, 112002 (2019).
[41] S. Acharya *et al.* (ALICE Collaboration), Exploring the NΛ-NΣ coupled system with high precision correlation techniques at the LHC, Phys. Lett. B **833**, 137272 (2022).
[42] S. Acharya *et al.* (ALICE Collaboration), Towards the understanding of the genuine three-body interaction for p-p-p and p-p-Λ, Eur. Phys. J. A **59**, 145 (2023).
[43] (ALICE Collaboration), Unveiling the strong interaction among hadrons at the LHC, Nature (London) **588**, 232 (2020); Nature (London) **590**, E13 (2021).
[44] L. Fabbietti, V. Mantovani Sarti, and O. Vazquez Doce, Study of the strong interaction among hadrons with correlations at the LHC, Annu. Rev. Nucl. Part. Sci. **71**, 377 (2021).
[45] A. Feliciello and T. Nagae, Experimental review of hypernuclear physics: Recent achievements and future perspectives, Rep. Prog. Phys. **78**, 096301 (2015).
[46] H. Tamura *et al.*, Gamma-ray spectroscopy of hypernuclei—present and future, Nucl. Phys. **A914**, 99 (2013).
[47] A. Gal, E. V. Hungerford, and D. J. Millener, Strangeness in nuclear physics, Rev. Mod. Phys. **88**, 035004 (2016).

[48] E. Friedman and A. Gal, Λ hypernuclear potentials beyond linear density dependence, Nucl. Phys. **A1039**, 122725 (2023).
[49] H. Le, J. Haidenbauer, U.-G. Meißner, and A. Nogga, Jacobi no-core shell model for *p*-shell hypernuclei, Eur. Phys. J. A **56**, 301 (2020).
[50] H. Le, J. Haidenbauer, U.-G. Meißner, and A. Nogga, *Ab initio* calculation of charge-symmetry breaking in $A = 7$ and 8 Λ hypernuclei, Phys. Rev. C **107**, 024002 (2023).
[51] H. Le, J. Haidenbauer, U.-G. Meißner, and A. Nogga, Separation energies of light Λ hypernuclei and their theoretical uncertainties, Eur. Phys. J. A **60**, 3 (2024).
[52] K. Hebeler, J. D. Holt, J. Menendez, and A. Schwenk, Nuclear forces and their impact on neutron-rich nuclei and neutron-rich matter, Annu. Rev. Nucl. Part. Sci. **65**, 457 (2015).
[53] J. E. Lynn, I. Tews, S. Gandolfi, and A. Lovato, Quantum Monte Carlo methods in nuclear physics: Recent advances, Annu. Rev. Nucl. Part. Sci. **69**, 279 (2019).
[54] H. Hergert, A guided tour of ab initio nuclear many-body theory, Front. Phys. **8**, 379 (2020).
[55] A. Rios, Green's function techniques for infinite nuclear systems, Front. Phys. **8**, 387 (2020).
[56] P. Demol, T. Duguet, A. Ekström, M. Frosini, K. Hebeler, S. König, D. Lee, A. Schwenk, V. Somà, and A. Tichai, Improved many-body expansions from eigenvector continuation, Phys. Rev. C **101**, 041302 (2020).
[57] C. Drischler, J. W. Holt, and C. Wellenhofer, Chiral effective field theory and the high-density nuclear equation of state, Annu. Rev. Nucl. Part. Sci. **71**, 403 (2021).
[58] A. Lovato, I. Bombaci, D. Logoteta, M. Piarulli, and R. B. Wiringa, Benchmark calculations of infinite neutron matter with realistic two- and three-nucleon potentials, Phys. Rev. C **105**, 055808 (2022).
[59] P. Arthuis, C. Barbieri, F. Pederiva, and A. Roggero, Quantum Monte Carlo calculations in configuration space with three-nucleon forces, Phys. Rev. C **107**, 044303 (2023).
[60] Y. Sekiguchi, K. Kiuchi, K. Kyutoku, and M. Shibata, Effects of hyperons in binary neutron star mergers, Phys. Rev. Lett. **107**, 211101 (2011).
[61] D. Radice, S. Bernuzzi, W. Del Pozzo, L. F. Roberts, and C. D. Ott, Probing extreme-density matter with gravitational wave observations of binary neutron star merger remnants, Astrophys. J. Lett. **842**, L10 (2017).
[62] N. K. Glendenning, Neutron stars are giant hypernuclei?, Astrophys. J. **293**, 470 (1985).
[63] B. D. Lackey, M. Nayyar, and B. J. Owen, Observational constraints on hyperons in neutron stars, Phys. Rev. D **73**, 024021 (2006).
[64] J. S. Read, B. D. Lackey, B. J. Owen, and J. L. Friedman, Constraints on a phenomenologically parameterized neutron-star equation of state, Phys. Rev. D **79**, 124032 (2009).
[65] K. Hotokezaka, K. Kyutoku, H. Okawa, M. Shibata, and K. Kiuchi, Binary neutron star mergers: Dependence on the nuclear equation of state, Phys. Rev. D **83**, 124008 (2011).
[66] A. Bauswein, H. T. Janka, K. Hebeler, and A. Schwenk, Equation-of-state dependence of the gravitational-wave signal from the ring-down phase of neutron-star mergers, Phys. Rev. D **86**, 063001 (2012).
[67] K. Takami, L. Rezzolla, and L. Baiotti, Spectral properties of the post-merger gravitational-wave signal from binary neutron stars, Phys. Rev. D **91**, 064001 (2015).
[68] S. Bernuzzi, T. Dietrich, and A. Nagar, Modeling the complete gravitational wave spectrum of neutron star mergers, Phys. Rev. Lett. **115**, 091101 (2015).
[69] T. Dietrich, M. Ujevic, W. Tichy, S. Bernuzzi, and B. Bruegmann, Gravitational waves and mass ejecta from binary neutron star mergers: Effect of the mass-ratio, Phys. Rev. D **95**, 024029 (2017).
[70] M. Hanauske, K. Takami, L. Bovard, L. Rezzolla, J. A. Font, F. Galeazzi, and H. Stöcker, Rotational properties of hypermassive neutron stars from binary mergers, Phys. Rev. D **96**, 043004 (2017).
[71] A. Feo, R. De Pietri, F. Maione, and F. Löffler, Modeling mergers of known galactic systems of binary neutron stars, Classical Quantum Gravity **34**, 034001 (2017).
[72] S. Vretinaris, N. Stergioulas, and A. Bauswein, Empirical relations for gravitational-wave asteroseismology of binary neutron star mergers, Phys. Rev. D **101**, 084039 (2020).
[73] A. Kedia, H. I. Kim, I.-S. Suh, and G. J. Mathews, Binary neutron star mergers as a probe of quark-hadron crossover equations of state, Phys. Rev. D **106**, 103027 (2022).
[74] C. A. Raithel and V. Paschalidis, Influence of stellar compactness on finite-temperature effects in neutron star merger simulations, Phys. Rev. D **108**, 083029 (2023).
[75] J. Antoniadis *et al.*, A massive pulsar in a compact relativistic binary, Science **340**, 6131 (2013).
[76] B. Margalit and B. D. Metzger, Constraining the maximum mass of neutron stars from multi-messenger observations of GW170817, Astrophys. J. Lett. **850**, L19 (2017).
[77] A. Bauswein, O. Just, H.-T. Janka, and N. Stergioulas, Neutron-star radius constraints from GW170817 and future detections, Astrophys. J. Lett. **850**, L34 (2017).
[78] M. Shibata, S. Fujibayashi, K. Hotokezaka, K. Kiuchi, K. Kyutoku, Y. Sekiguchi, and M. Tanaka, Modeling GW170817 based on numerical relativity and its implications, Phys. Rev. D **96**, 123012 (2017).
[79] M. Ruiz, S. L. Shapiro, and A. Tsokaros, GW170817, General relativistic magnetohydrodynamic simulations, and the neutron star maximum mass, Phys. Rev. D **97**, 021501 (2018).
[80] D. Radice, A. Perego, F. Zappa, and S. Bernuzzi, GW170817: Joint constraint on the neutron star equation of state from multimessenger observations, Astrophys. J. Lett. **852**, L29 (2018).
[81] E. R. Most, L. J. Papenfort, V. Dexheimer, M. Hanauske, S. Schramm, H. Stöcker, and L. Rezzolla, Signatures of quark-hadron phase transitions in general-relativistic neutron-star mergers, Phys. Rev. Lett. **122**, 061101 (2019).
[82] L. Rezzolla, E. R. Most, and L. R. Weih, Using gravitational-wave observations and quasi-universal relations to constrain the maximum mass of neutron stars, Astrophys. J. Lett. **852**, L25 (2018).
[83] S. Köppel, L. Bovard, and L. Rezzolla, A general-relativistic determination of the threshold mass to prompt collapse in binary neutron star mergers, Astrophys. J. Lett. **872**, L16 (2019).

[84] B. P. Abbott *et al.* (LIGO Scientific and Virgo Collaborations), Properties of the binary neutron star merger GW170817, Phys. Rev. X **9**, 011001 (2019).

[85] T. E. Riley *et al.*, A *NICER* view of PSR J0030 + 0451: Millisecond pulsar parameter estimation, Astrophys. J. Lett. **887**, L21 (2019).

[86] M. C. Miller *et al.*, PSR J0030 + 0451 mass and radius from *NICER* data and implications for the properties of neutron star matter, Astrophys. J. Lett. **887**, L24 (2019).

[87] D. Radice and L. Dai, Multimessenger parameter estimation of GW170817, Eur. Phys. J. A **55**, 50 (2019).

[88] M. W. Coughlin, T. Dietrich, B. Margalit, and B. D. Metzger, Multimessenger Bayesian parameter inference of a binary neutron star merger, Mon. Not. R. Astron. Soc. **489**, L91 (2019).

[89] T. Dietrich, M. W. Coughlin, P. T. H. Pang, M. Bulla, J. Heinzel, L. Issa, I. Tews, and S. Antier, Multimessenger constraints on the neutron-star equation of state and the Hubble constant, Science **370**, 1450 (2020).

[90] C. D. Capano, I. Tews, S. M. Brown, B. Margalit, S. De, S. Kumar, D. A. Brown, B. Krishnan, and S. Reddy, Stringent constraints on neutron-star radii from multimessenger observations and nuclear theory, Nat. Astron. **4**, 625 (2020).

[91] T. E. Riley *et al.*, A NICER view of the massive pulsar PSR J0740 + 6620 informed by radio timing and XMM-Newton spectroscopy, Astrophys. J. Lett. **918**, L27 (2021).

[92] M. C. Miller *et al.*, The radius of PSR J0740 + 6620 from NICER and XMM-Newton data, Astrophys. J. Lett. **918**, L28 (2021).

[93] M. Al-Mamun, A. W. Steiner, J. Nättilä, J. Lange, R. O'Shaughnessy, I. Tews, S. Gandolfi, C. Heinke, and S. Han, Combining electromagnetic and gravitational-wave constraints on neutron-star masses and radii, Phys. Rev. Lett. **126**, 061101 (2021).

[94] G. Raaijmakers, S. K. Greif, K. Hebeler, T. Hinderer, S. Nissanke, A. Schwenk, T. E. Riley, A. L. Watts, J. M. Lattimer, and W. C. G. Ho, Constraints on the dense matter equation of state and neutron star properties from NICER's Mass–radius estimate of PSR J0740 + 6620 and multimessenger observations, Astrophys. J. Lett. **918**, L29 (2021).

[95] M. Breschi, A. Perego, S. Bernuzzi, W. Del Pozzo, V. Nedora, D. Radice, and D. Vescovi, AT2017gfo: Bayesian inference and model selection of multicomponent kilonovae and constraints on the neutron star equation of state, Mon. Not. R. Astron. Soc. **505**, 1661 (2021).

[96] E. Fonseca *et al.*, Refined mass and geometric measurements of the high-mass PSR J0740 + 6620, Astrophys. J. Lett. **915**, L12 (2021).

[97] R. W. Romani, D. Kandel, A. V. Filippenko, T. G. Brink, and W. Zheng, PSR J0952-0607: The fastest and heaviest known galactic neutron star, Astrophys. J. Lett. **934**, L17 (2022).

[98] S. Huth *et al.*, Constraining neutron-star matter with microscopic and macroscopic collisions, Nature (London) **606**, 276 (2022).

[99] C. Huang, G. Raaijmakers, A. L. Watts, L. Tolos, and C. Providência, Constraining fundamental nuclear physics parameters using neutron star mass-radius measurements I: Nucleonic models, arXiv:2303.17518.

[100] R. Oechslin, S. Rosswog, and F. K. Thielemann, Conformally flat smoothed particle hydrodynamics: Application to neutron star mergers, Phys. Rev. D **65**, 103005 (2002).

[101] R. Oechslin, H. T. Janka, and A. Marek, Relativistic neutron star merger simulations with non-zero temperature equations of state. 1. Variation of binary parameters and equation of state, Astron. Astrophys. **467**, 395 (2007).

[102] A. Bauswein, R. Oechslin, and H. T. Janka, Discriminating strange star mergers from neutron star mergers by gravitational-wave measurements, Phys. Rev. D **81**, 024012 (2010).

[103] J. Isenberg and J. Nester, Canonical gravity, in *General Relativity and Gravitation. Vol. 1. One Hundred Years After the Birth of Albert Einstein*, edited by A. Held (Plenum Press, New York, 1980), p. 23.

[104] J. R. Wilson, G. J. Mathews, and P. Marronetti, Relativistic numerical model for close neutron star binaries, Phys. Rev. D **54**, 1317 (1996).

[105] S. Banik, M. Hempel, and D. Bandyopadhyay, New hyperon equations of state for supernovae and neutron stars in density-dependent hadron field theory, Astrophys. J. Suppl. Ser. **214**, 22 (2014).

[106] M. Marques, M. Oertel, M. Hempel, and J. Novak, New temperature dependent hyperonic equation of state: Application to rotating neutron star models and *I*-*Q* relations, Phys. Rev. C **96**, 045806 (2017).

[107] V. Dexheimer, Tabulated neutron star equations of state modeled within the chiral mean field model, Pub. Astron. Soc. Aust. **34**, E006 (2017).

[108] H. Kochankovski, A. Ramos, and L. Tolos, Equation of state for hot hyperonic neutron star matter, Mon. Not. R. Astron. Soc. **517**, 507 (2022); H. Kochankovski, A. Ramos, and L. TolosMon. Not. R. Astron. Soc. **518**, 6376(E) (2022).

[109] J. R. Stone, V. Dexheimer, P. A. M. Guichon, A. W. Thomas, and S. Typel, Equation of state of hot dense hyperonic matter in the quark–meson-coupling (QMC-A) model, Mon. Not. R. Astron. Soc. **502**, 3476 (2021).

[110] M. Fortin, M. Oertel, and C. Providência, Hyperons in hot dense matter: What do the constraints tell us for equation of state?, Pub. Astron. Soc. Aust. **35**, 44 (2018).

[111] H. Kochankovski, A. Ramos, and L. Tolos, Hyperonic uncertainties in neutron stars, mergers and supernovae, Mon. Not. R. Astron. Soc. **528**, 2629 (2024).

[112] A. Akmal, V. R. Pandharipande, and D. G. Ravenhall, The Equation of state of nucleon matter and neutron star structure, Phys. Rev. C **58**, 1804 (1998).

[113] A. S. Schneider, C. Constantinou, B. Muccioli, and M. Prakash, Akmal-Pandharipande-Ravenhall equation of state for simulations of supernovae, neutron stars, and binary mergers, Phys. Rev. C **100**, 025803 (2019).

[114] S. Typel, G. Ropke, T. Klahn, D. Blaschke, and H. H. Wolter, Composition and thermodynamics of nuclear matter with light clusters, Phys. Rev. C **81**, 015803 (2010).

[115] M. Hempel and J. Schaffner-Bielich, Statistical model for a complete supernova equation of state, Nucl. Phys. **A837**, 210 (2010).

[116] D. Alvarez-Castillo, A. Ayriyan, S. Benic, D. Blaschke, H. Grigorian, and S. Typel, New class of hybrid EoS and Bayesian M-R data analysis, Eur. Phys. J. A **52**, 69 (2016).
[117] S. Furusawa, H. Togashi, H. Nagakura, K. Sumiyoshi, S. Yamada, H. Suzuki, and M. Takano, A new equation of state for core-collapse supernovae based on realistic nuclear forces and including a full nuclear ensemble, J. Phys. G **44**, 094001 (2017).
[118] H. Togashi, K. Nakazato, Y. Takehara, S. Yamamuro, H. Suzuki, and M. Takano, Nuclear equation of state for core-collapse supernova simulations with realistic nuclear forces, Nucl. Phys. **A961**, 78 (2017).
[119] G. Shen, C. J. Horowitz, and S. Teige, A new equation of state for astrophysical simulations, Phys. Rev. C **83**, 035802 (2011).
[120] I. Bombaci and D. Logoteta, Equation of state of dense nuclear matter and neutron star structure from nuclear chiral interactions, Astron. Astrophys. **609**, A128 (2018).
[121] D. Logoteta, A. Perego, and I. Bombaci, Microscopic equation of state of hot nuclear matter for numerical relativity simulations, Astron. Astrophys. **646**, A55 (2021).
[122] J. M. Lattimer and F. D. Swesty, A generalized equation of state for hot, dense matter, Nucl. Phys. **A535**, 331 (1991).
[123] A. W. Steiner, M. Hempel, and T. Fischer, Core-collapse supernova equations of state based on neutron star observations, Astrophys. J. **774**, 17 (2013).
[124] E. Chabanat, P. Bonche, P. Haensel, J. Meyer, and R. Schaeffer, A Skyrme parametrization from subnuclear to neutron star densities. 2. Nuclei far from stablities, Nucl. Phys. **A635**, 231 (1998); Nucl. Phys. **A643**, 441 (E) (1998).
[125] A. S. Schneider, L. F. Roberts, and C. D. Ott, Open-source nuclear equation of state framework based on the liquid-drop model with Skyrme interaction, Phys. Rev. C **96**, 065802 (2017).
[126] Y. Sugahara and H. Toki, Relativistic mean field theory for unstable nuclei with nonlinear sigma and omega terms, Nucl. Phys. **A579**, 557 (1994).
[127] M. Hempel, T. Fischer, J. Schaffner-Bielich, and M. Liebendorfer, New equations of state in simulations of core-collapse supernovae, Astrophys. J. **748**, 70 (2012).
[128] H. Toki, D. Hirata, Y. Sugahara, K. Sumiyoshi, and I. Tanihata, Relativistic many body approach for unstable nuclei and supernova, Nucl. Phys. **A588**, c357 (1995).
[129] X. Du, A. W. Steiner, and J. W. Holt, Hot and dense matter equation of state probability distributions for astrophysical simulations, Phys. Rev. C **105**, 035803 (2022).
[130] S. Typel, M. Oertel, and T. Klähn, CompOSE CompStar online supernova equations of state harmonising the concert of nuclear physics and astrophysics compose.obspm.fr, Phys. Part. Nucl. **46**, 633 (2015).
[131] S. Typel *et al.* (CompOSE Core Team Collaboration), CompOSE reference manual, Eur. Phys. J. A **58**, 221 (2022).
[132] B. P. Abbott *et al.* (LIGO Scientific and Virgo Collaborations), GW170817: Observation of gravitational waves from a binary neutron star inspiral, Phys. Rev. Lett. **119**, 161101 (2017).
[133] S. De, D. Finstad, J. M. Lattimer, D. A. Brown, E. Berger, and C. M. Biwer, Tidal deformabilities and radii of neutron stars from the observation of GW170817, Phys. Rev. Lett. **121**, 091102 (2018); Phys. Rev. Lett. **121**, 259902(E) (2018).
[134] B. P. Abbott *et al.* (LIGO Scientific and Virgo Collaborations), GW170817: Measurements of neutron star radii and equation of state, Phys. Rev. Lett. **121**, 161101 (2018).
[135] H. T. Janka, T. Zwerger, and R. Moenchmeyer, Does artificial viscosity destroy prompt type-II supernova explosions?, Astron. Astrophys. **268**, 360 (1993), https://articles.adsabs.harvard.edu/pdf/1993A%26A...268..360J.
[136] C. Constantinou, B. Muccioli, M. Prakash, and J. M. Lattimer, Thermal properties of hot and dense matter with finite range interactions, Phys. Rev. C **92**, 025801 (2015).
[137] A. Bauswein, H. T. Janka, and R. Oechslin, Testing approximations of thermal effects in neutron star merger simulations, Phys. Rev. D **82**, 084043 (2010).
[138] C. Raithel, V. Paschalidis, and F. Özel, Realistic finite-temperature effects in neutron star merger simulations, Phys. Rev. D **104**, 063016 (2021).
[139] J. Fields, A. Prakash, M. Breschi, D. Radice, S. Bernuzzi, and A. da Silva Schneider, Thermal effects in binary neutron star mergers, Astrophys. J. Lett. **952**, L36 (2023).
[140] J. Clark, A. Bauswein, L. Cadonati, H. T. Janka, C. Pankow, and N. Stergioulas, Prospects for high frequency burst searches following binary neutron star coalescence with advanced gravitational wave detectors, Phys. Rev. D **90**, 062004 (2014).
[141] K. Chatziioannou, J. A. Clark, A. Bauswein, M. Millhouse, T. B. Littenberg, and N. Cornish, Inferring the post-merger gravitational wave emission from binary neutron star coalescences, Phys. Rev. D **96**, 124035 (2017).
[142] H. Yang, V. Paschalidis, K. Yagi, L. Lehner, F. Pretorius, and N. Yunes, Gravitational wave spectroscopy of binary neutron star merger remnants with mode stacking, Phys. Rev. D **97**, 024049 (2018).
[143] A. Torres-Rivas, K. Chatziioannou, A. Bauswein, and J. A. Clark, Observing the post-merger signal of GW170817-like events with improved gravitational-wave detectors, Phys. Rev. D **99**, 044014 (2019).
[144] K. W. Tsang, T. Dietrich, and C. Van Den Broeck, Modeling the postmerger gravitational wave signal and extracting binary properties from future binary neutron star detections, Phys. Rev. D **100**, 044047 (2019).
[145] P. J. Easter, S. Ghonge, P. D. Lasky, A. R. Casey, J. A. Clark, F. H. Vivanco, and K. Chatziioannou, Detection and parameter estimation of binary neutron star merger remnants, Phys. Rev. D **102**, 043011 (2020).
[146] M. Breschi, R. Gamba, S. Borhanian, G. Carullo, and S. Bernuzzi, Kilohertz gravitational waves from binary neutron star mergers: Inference of postmerger signals with the Einstein telescope, arXiv:2205.09979.
[147] M. Wijngaarden, K. Chatziioannou, A. Bauswein, J. A. Clark, and N. J. Cornish, Probing neutron stars with the full premerger and postmerger gravitational wave signal from binary coalescences, Phys. Rev. D **105**, 104019 (2022).
[148] A. W. Criswell, J. Miller, N. Woldemariam, T. Soultanis, A. Bauswein, K. Chatziioannou, M. W. Coughlin, G. Jones, and V. Mandic, Hierarchical Bayesian method for constraining the neutron star equation of state with an

ensemble of binary neutron star postmerger remnants, Phys. Rev. D **107**, 043021 (2023).
[149] A. Bauswein, N. Stergioulas, and H.-T. Janka, Exploring properties of high-density matter through remnants of neutron-star mergers, Eur. Phys. J. A **52**, 56 (2016).
[150] E. E. Flanagan and T. Hinderer, Constraining neutron star tidal Love numbers with gravitational wave detectors, Phys. Rev. D **77**, 021502 (2008).
[151] T. Hinderer, Tidal Love numbers of neutron stars, Astrophys. J. **677**, 1216 (2008).
[152] T. Hinderer, B. D. Lackey, R. N. Lang, and J. S. Read, Tidal deformability of neutron stars with realistic equations of state and their gravitational wave signatures in binary inspiral, Phys. Rev. D **81**, 123016 (2010).
[153] T. Damour and A. Nagar, Effective one body description of tidal effects in inspiralling compact binaries, Phys. Rev. D **81**, 084016 (2010).
[154] T. Damour, A. Nagar, and L. Villain, Measurability of the tidal polarizability of neutron stars in late-inspiral gravitational-wave signals, Phys. Rev. D **85**, 123007 (2012).
[155] K. Chatziioannou, Neutron star tidal deformability and equation of state constraints, Gen. Relativ. Gravit. **52**, 109 (2020).
[156] T. Dietrich, T. Hinderer, and A. Samajdar, Interpreting binary neutron star mergers: Describing the binary neutron star dynamics, modelling gravitational waveforms, and analyzing detections, Gen. Relativ. Gravit. **53**, 27 (2021).
[157] G. Lioutas, A. Bauswein, and N. Stergioulas, Frequency deviations in universal relations of isolated neutron stars and postmerger remnants, Phys. Rev. D **104**, 043011 (2021).
[158] S. Blacker, N.-U. F. Bastian, A. Bauswein, D. B. Blaschke, T. Fischer, M. Oertel, T. Soultanis, and S. Typel, Constraining the onset density of the hadron-quark phase transition with gravitational-wave observations, Phys. Rev. D **102**, 123023 (2020).
[159] J. Keller, C. Wellenhofer, K. Hebeler, and A. Schwenk, Neutron matter at finite temperature based on chiral effective field theory interactions, Phys. Rev. C **103**, 055806 (2021).
[160] J. Keller, K. Hebeler, and A. Schwenk, Nuclear equation of state for arbitrary proton fraction and temperature based on chiral effective field theory and a Gaussian process emulator, Phys. Rev. Lett. **130**, 072701 (2023).
[161] S. Huth, C. Wellenhofer, and A. Schwenk, New equations of state constrained by nuclear physics, observations, and QCD calculations of high-density nuclear matter, Phys. Rev. C **103**, 025803 (2021).
[162] G. A. Lalazissis, T. Niksic, D. Vretenar, and P. Ring, New relativistic mean-field interaction with density-dependent meson-nucleon couplings, Phys. Rev. C **71**, 024312 (2005).
[163] A. Sedrakian and A. Harutyunyan, Delta-resonances and hyperons in proto-neutron stars and merger remnants, Eur. Phys. J. A **58**, 137 (2022).
[164] G. Fiorella Burgio and A. F. Fantina, Nuclear equation of state for compact stars and supernovae, Astrophysics and Space Science Library **457**, 255 (2018).
[165] M. Durante *et al.*, All the fun of the FAIR: Fundamental physics at the facility for antiproton and ion research, Phys. Scr. **94**, 033001 (2019).
[166] K. Hebeler, Three-nucleon forces: Implementation and applications to atomic nuclei and dense matter, Phys. Rep. **890**, 1 (2021).
[167] S. Petschauer, J. Haidenbauer, N. Kaiser, U.-G. Meißner, and W. Weise, Hyperon-nuclear interactions from SU(3) chiral effective field theory, Front. Phys. **8**, 12 (2020).
[168] J. Haidenbauer, U.-G. Meißner, A. Nogga, and H. Le, Hyperon–nucleon interaction in chiral effective field theory at next-to-next-to-leading order, Eur. Phys. J. A **59**, 63 (2023).
[169] R. Wirth, D. Gazda, P. Navrátil, and R. Roth, Hypernuclear no-core shell model, Phys. Rev. C **97**, 064315 (2018).
[170] R. Wirth and R. Roth, Similarity renormalization group evolution of hypernuclear Hamiltonians, Phys. Rev. C **100**, 044313 (2019).
[171] M. Prakash, M. Prakash, J. M. Lattimer, and C. J. Pethick, Rapid cooling of neutron stars by hyperons and Delta isobars, Astrophys. J. Lett. **390**, L77 (1992).
[172] D. Page, J. M. Lattimer, M. Prakash, and A. W. Steiner, Minimal cooling of neutron stars: A new paradigm, Astrophys. J. Suppl. Ser. **155**, 623 (2004).
[173] D. G. Yakovlev and C. J. Pethick, Neutron star cooling, Annu. Rev. Astron. Astrophys. **42**, 169 (2004).
[174] K. Sumiyoshi, C. Ishizuka, A. Ohnishi, S. Yamada, and H. Suzuki, Emergence of hyperons in failed supernovae: Trigger of the black hole formation, Astrophys. J. Lett. **690**, L43 (2009).
[175] K. Nakazato, S. Furusawa, K. Sumiyoshi, A. Ohnishi, S. Yamada, and H. Suzuki, Hyperon matter and black hole formation in failed supernovae, Astrophys. J. **745**, 197 (2012).
[176] B. Peres, M. Oertel, and J. Novak, Influence of pions and hyperons on stellar black hole formation, Phys. Rev. D **87**, 043006 (2013).
[177] S. Banik, Probing the metastability of a protoneutron star with hyperons in a core-collapse supernova, Phys. Rev. C **89**, 035807 (2014).
[178] A. R. Raduta, A. Sedrakian, and F. Weber, Cooling of hypernuclear compact stars, Mon. Not. R. Astron. Soc. **475**, 4347 (2018).
[179] R. Negreiros, L. Tolos, M. Centelles, A. Ramos, and V. Dexheimer, Cooling of small and massive hyperonic stars, Astrophys. J. **863**, 104 (2018).
[180] H. Grigorian, D. N. Voskresensky, and K. A. Maslov, Cooling of neutron stars in "nuclear medium cooling scenario" with stiff equation of state including hyperons, Nucl. Phys. **A980**, 105 (2018).
[181] A. R. Raduta, J. J. Li, A. Sedrakian, and F. Weber, Cooling of hypernuclear compact stars: Hartree–Fock models and high-density pairing, Mon. Not. R. Astron. Soc. **487**, 2639 (2019).
[182] T. Malik and C. Providência, Bayesian inference of signatures of hyperons inside neutron stars, Phys. Rev. D **106**, 063024 (2022).

[183] M. Fortin, A. R. Raduta, S. Avancini, and C. Providência, Thermal evolution of relativistic hyperonic compact stars with calibrated equations of state, Phys. Rev. D **103**, 083004 (2021).

[184] A. Bauswein, N. Stergioulas, and H. T. Janka, Revealing the high-density equation of state through binary neutron star mergers, Phys. Rev. D **90**, 023002 (2014).

[185] A. Bauswein, N.-U. Friedrich Bastian, D. Blaschke, K. Chatziioannou, J. A. Clark, T. Fischer, H.-T. Janka, O. Just, M. Oertel, and N. Stergioulas, Equation-of-state constraints and the QCD phase transition in the era of gravitational-wave astronomy, AIP Conf. Proc. **2127**, 020013 (2019).

[186] L. R. Weih, M. Hanauske, and L. Rezzolla, Postmerger gravitational-wave signatures of phase transitions in binary mergers, Phys. Rev. Lett. **124**, 171103 (2020).

[187] A. Bauswein and S. Blacker, Impact of quark deconfinement in neutron star mergers and hybrid star mergers, Eur. Phys. J. ST **229**, 3595 (2020).

[188] S. L. Liebling, C. Palenzuela, and L. Lehner, Effects of high density phase transitions on neutron star dynamics, Classical Quantum Gravity **38**, 115007 (2021).

[189] A. Prakash, D. Radice, D. Logoteta, A. Perego, V. Nedora, I. Bombaci, R. Kashyap, S. Bernuzzi, and A. Endrizzi, Signatures of deconfined quark phases in binary neutron star mergers, Phys. Rev. D **104**, 083029 (2021).

[190] V. Vijayan, N. Rahman, A. Bauswein, G. Martínez-Pinedo, and I. L. Arbina, Impact of pions on binary neutron star mergers, Phys. Rev. D **108**, 023020 (2023).